An experimental study on a wake of a torus body using UVP monitor

Authors: **Yoshihiro Inoue[1], Shintaro Yamashita[2], and Masaya Kumada[2]**

Institution: Department of Mechanical Engineering, Suzuka College of Technology

Running head: Y. Inoue et al. / A wake of a torus body

Titles and Address: [1] Department of Mechanical Engineering, Suzuka College of Technology, Suzuka, Mie 510-02, Japan

[2] Department of Mechanical Engineering, Gifu University, Gifu 501-11, Japan

Abstract. A flow around a torus body has a complicated three-dimensional structure, and it is difficult in this flow to measure a spatiotemporal field of velocity by means of conventional methods such as hot-wire anemometers. In this study, the wakes of the tori with the diameter ratio of 3 and 5 are investigated in an axisymmetric and oblique postures mainly for the Reynolds number of 1500. The vortical structures are observed by the flow visualization techniques, and instantaneous velocity profiles in the x- and y-directions are measured with an ultrasonic velocity profile monitor (UVP). The time history of the instantaneous velocity profile is presented, and the spatial distribution of power-spectrum and two-point correlation coefficient are analyzed. A system for multi-line measurements of the UVP is developed, and a velocity field conditionally averaged for vortex shedding is shown.

List of symbols

D	center-line diameter
d	cross-sectional diameter
R_{11}	correlation coefficient
Re	Reynolds number
r_x	streamwise spacing between two points
St	Strouhal number
U_0	mainstream velocity
U_c	convection velocity

U, V	mean velocity components in the x- and y-directions
u, v	fluctuating velocity components
$\tilde{u}$, $\tilde{v}$	instantaneous velocity components
u', v'	rms values of fluctuating velocity
x	distance in the mainstream direction
y	distance parallel to the symmetry plane of the flow and normal to the x-axis
x_{tr}, y_{tr}	position of the transducer tip
α_{tr}	angle between the measuring line and x-axis
θ	oblique angle of the torus against the mainstream
ω_z	vorticity

1 Introduction

Flows around a three-dimensional bluff body and three-dimensional separated flows are of great interest in the field of fluid mechanics. The vortex formation process even in a wake of a two-dimensional bluff body like a straight cylinder (Williamson, 1995), however, is not made clear yet, because of its three-dimensionality and unsteadiness. Many difficult problems related to the flow structure in the near wake remain to be solved. Axisymmetric bluff bodies have received attention from many investigators for their simple geometrical shape and wide variety of practical applications: for example, a disk (Calvert, 1967; Higuchi et al., 1996), a sphere (Sakamoto and Haniu, 1990) and a ring (Takamoto, 1987; Miau et al., 1992). On the other hand, a body of revolution at an angle of attack in a uniform flow has been also investigated to understand the topology of three-dimensional separated flow (Tobak and Peake, 1982).

In the present study, the structure of a wake behind a torus body has been investigated; the torus is a ring with a circular cross-section. This flow is a basic one applicable to many problems, including bio-fluid mechanics for DNA polymer, properties of flow with micelles, and the drag and heat transfer performance for helical heating tubes.

The flow around the torus has a three-dimensional complicated structure, and so far few studies have been made from the engineering and fundamental points of view. Monson (1983), who made free-fall experiments with different tori in a viscous fluid, found the drag data in the viscous regime and a variety of flow patterns against a projected area solidity. Also, Amarakoon et al. (1982) obtained

the drag on the torus falling in a viscous liquid contained by tanks of different cross-sections. In analytical studies for low Reynolds numbers, Johnson and Wu (1979) employed a singularity method for Stokes flow and obtained force coefficients for various motions of the torus. Goren and O'Neill (1980) solved exactly the equations of creeping fluid motion using toroidal coordinates and computed the resisting forces for toroids with various solidities.

Recently, Leweke and Provansal (1995) investigated the wakes behind four rings with different aspect ratios in a wind tunnel. They yielded the Strouhal curves in the periodic regime and transition range, and identified the periodic vortex shedding modes, that is, the parallel mode and helical oblique modes. Furthermore, they studied the ring wake using a dynamical wake model involving a Ginzburg-Landau amplitude equation and compared its predictions with their experimental data.

Our present experiments were carried out in a water channel using a flow visualization technique and an ultrasonic Doppler method. The ultrasonic velocity profile (UVP) monitor developed by Takeda (1995) yields spatiotemporal information on the velocity, so that the wake structure of the torus is made clear in this study, both in the cases of a zero inclination and oblique postures of the torus.

2 Experimental methods

2.1 Test rig

Experiments were performed in a free-surface water channel. Water preserved in the underground pit is pumped up and introduced through a control valve into the channel. The flow settled by means of a straightener and screens is contracted into a test section. The layout around the test channel is shown in Fig. 1. The channel is 700 mm wide, 3 m long, and 500 mm deep at the top of the weir. The torus body is suspended on a circular rod, whose other end is fixed at a rotatable table on the channel, in the middle of a cross section 1 m downstream from the contraction end. An ultrasound transducer is held in a tip of a streamline-shaped support, which is fastened to a traversing device.

The flow field and coordinate system are shown in Fig. 2. The cross-sectional diameter and center-line diameter of the torus body are defined as d and D, respectively. A ratio D/d is a geometrical parameter of the torus, and in this study the cases of $D/d = 3$ and 5 with $d = 30$ mm are investigated. An inclination of the symmetry axis of torus to the mainstream direction presents an attitude of the torus. The oblique angle θ was varied in the range of 0° to 85°, and the zero inclination, that is $\theta = 0$, is an axisymmetric posture. A dynamical parameter of the flow is the Reynolds number, which is

based on a free stream velocity U_0 and the cross-sectional diameter d in the present study. The free stream velocity remains constant at 50 mm/s, and the Reynolds number Re is nearly equal to 1500. The origin of co-ordinates is on a plane of symmetry of the torus body and at the center of its rim, and the x-axis is taken to be coincident with the mainstream direction. The flow visualization by a hydrogen-bubble technique and measurements with the UVP monitor were made on the symmetry plane of the flow, i.e., the x-y plane.

2.2 UVP monitor and multiplexer

The UVP monitor used in this study is a model X3-PS (Met-Flow). The hydrogen bubbles, which were generated and seeded from a cathode wire by the electrolysis of water, were utilized as particles reflecting the ultrasound. The cathode wire is a platinum wire of 20 μm diameter and positioned upstream of the torus, as shown in Fig. 1.

A basic frequency of the ultrasonic transducer is 4 MHz (IMASONIC), and the other measuring parameters are shown in Table 1. The arrangement of the ultrasound transducer is shown in Fig. 2. A location and orientation of measuring line are presented in terms of the position of the transducer tip, x_{tr} and y_{tr}, and of an angle from the x-axis, α_{tr}. Therefore, the velocity $\tilde{q}$ instantaneously detected by the UVP monitor is a function of α_{tr},

$$\tilde{q}(x_i, y_i) = \tilde{u}(x_i, y_i) \cos \alpha_{tr} + \tilde{v}(x_i, y_i) \sin \alpha_{tr}, \tag{1}$$

and the measuring positions are

$$\begin{aligned} x_i &= x_{tr} + (\xi_{st} + \xi_{ch}\, i) \cos \alpha_{tr}, \\ y_i &= y_{tr} + (\xi_{st} + \xi_{ch}\, i) \sin \alpha_{tr} \quad (i = 0, 1, \cdots, 127), \end{aligned} \tag{2}$$

where ξ_{st} and ξ_{ch} are the starting depth and channel distance of the UVP monitor, respectively. The transducer arrangements and spatial measuring parameters adopted in this experiment are also listed in Table 1.

A multi-measurement system applied to conditionally averaging the velocity profiles is shown schematically in Fig. 3, and a setting of a reference transducer is given in the last column of Table 1. Two transducers are alternately switched by a multiplexer (64-System, JcAIR), which is controlled together with the UVP monitor by a personal computer (FMV-Series, FUJITSU). The time period of the transducer switching is 145 ms.

3 Results and discussion

3.1 Axisymmetric wake at zero inclination

Flow visualization and vortex shedding frequency

The flows visualized by a hydrogen-bubble method are shown in Fig. 4. Mean flow fields for D/d = 3 and 5 are axisymmetric, but the vortical structures for these flows are different from each other. In the near wake region of $D/d = 5$, say within about 1 D downstream of the torus, the inside and outside shear layers roll up alternately; they are separated from the caliber and circumference of the torus, respectively, and the vortex rings are shed downstream. In the case of $D/d = 3$, however, no vortex ring is discernible in this visualization picture, and the periodic variation of the velocity is rather observed near the axis of symmetry of the torus.

There is a dominant frequency of the fluctuating velocity in the wake of the torus at the zero inclination, probably corresponding to the vortex shedding. In order to estimate the dominant frequencies, measurements of the fluctuating velocity were made in a range of $600 < Re < 2700$ at x = 150 mm, where the inside and outside cylindrical shear layers separated from the torus roll up and periodic vortex structures are observed, as shown in Fig. 4. The variation in the vortex shedding frequency, represented in the Strouhal number $St = f\,d\,/\,U_0$, against the diameter ratio is shown in Fig. 5; the present data are for $Re \approx 1500$, and compared with rings having a sharp-edged cross-section (Takamoto, 1987) and two circular cylinders (Bearman and Wadcock, 1973). Takamoto (1987) has suggested in his investigations of the rings that there exists a structural change of the wake between D/d = 4.5 and 5.0. Monson (1983) also found that the patterns of the torus wake may be classified into three categories by the projected area solidity, $S = 4\,(D/d)\,/\,(D/d + 1)^2$, and that there is a sudden change between two flow patterns at $S \approx 0.6$ ($D/d \approx 4.4$). In the present experiments the tori with D/d = 3 and 5 were used; on referring to the above studies, the former corresponds to a disk mode which has an oblique loop wake structure typically generated by solid bodies, and the latter to a ring wake mode which consists of coherent axisymmetric structures. The vortex shedding frequencies for the torus were almost similar to the wake of two circular cylinders, and they remained almost unchanged for both regimes of the torus wake. No discrepancy seems to explicitly appear between the two wake modes in the shedding frequency in contrast to the wake of the ring model. In the wake of the torus with D/d = 3, however, the peak of the power spectrum is relatively smaller and much broader than that with D/d =5.

Figure 6 shows the change in the dominant frequencies with respect to the Reynolds number for the ring wake mode ($D/d = 5$) together with the results measured by Leweke and Provansal (1995) in the wake of the torus with $D/d = 10$. Leweke et al. have found from their careful experiments that transition from a stationary to an oscillating wake occurs at $Re \approx 50$, and that there are a periodic regime nearly in the interval $50 < Re < 190$ and a transition regime in $180 < Re < 350$. The Reynolds numbers in the present experiments are slightly above the transition regime, and by reference to the wake of a circular cylinder (Williamson, 1995), flows in this interval seem to be associated with a disorganized motion by a fine-scale three-dimensionality. It is observed from our results that the Strouhal number is nearly constant and slightly decreases as the Reynolds number increases above 1000. This behavior is probably the same for the circular cylinder (Blevins, 1995).

Spatiotemporal velocity field

Figures 7(a) and (b) show time histories of the instantaneous profile of the velocity component $\tilde{u}$ in the x-direction. The radial distances of measuring lines which are parallel to the x-axis are 30 mm and 50 mm for the diameter ratio of 3 and 5, respectively, and these positions nearly correspond to the inside separated shear layers. In the case of $D/d = 5$, the regions of higher and lower velocities appear alternatively and regularly in the time and/or streamwise directions and transfer linearly in the x-t plane. This slope indicates a convection velocity of flow structure, and the value estimated here in this case is 0.80 times the free stream velocity U_0. On the other hand, for $D/d = 3$, the regularity of the flow structure is found downstream of about $x = 150$ mm, and the convection velocity is smaller than that for $D/d = 5$.

Spatiotemporal contour maps of the instantaneous velocity component in the y-direction are shown in Figs. 8(a), (b) at $x = 150$ mm and Figs. 8(c), (d) at $x = 300$ mm; the abscissae denote the time and the ordinates are the lateral distance. The figures clearly show the flow patterns in the space-time field, in which the flow direction is right to left. The map for $D/d = 5$ at $x = 150$ mm (Fig. 8(b)) shows clearly the anti-symmetric contour patterns; thus the flow is symmetric with respect to $y = 0$, and the regions of the positive and negative velocities are arrayed with a spatiotemporally regular pattern. In the near field at $D/d = 3$ (Fig. 8(a)), there is a flow toward the center axis in the outer shear layer, and the regions of the positive and negative velocities are scattered about $y \approx \pm 40$ mm temporally. In the downstream position, $x = 300$ mm for $D/d = 5$ (Fig. 8(d)), it can be seen that the

regular patterns are clear and the structural arrangement of the flow remains almost unchanged both in the time and lateral directions. On the other hand, at $D/d = 3$ (Fig. 8(c)), a flow pattern is considerably altered compared with the upstream cross section; the regions of the positive and negative velocities become larger bulks than at the upstream position due to an absorption of the vortices and have a tendency to be located about $y = 0$. It seems that this modification of the velocity profile is connected with the transition of the flow structure from the cylindrical vortex to the vortex loop (see also in Fig. 4(a)), which was suggested by Sakamoto and Haniu (1990) for a wake of a sphere.

Flow structure

The space correlation of fluctuating velocities at two points separated in the main flow direction is useful for a structural analysis of flow, while its measurement is difficult by means of the method of hot-wires, because the upstream probe greatly disturbs the flow. For this reason, the UVP monitor has an advantage over the other velocity measurement methods and can measure such quantities without error due to the probe-induced disturbance.

The coefficient of space correlation is defined as,

$$R_{11}(x, y; r_x, r_y, \tau) = \frac{\overline{u(x, y; 0, 0, 0)\ u(x, y; r_x, r_y, \tau)}}{u'(x, y; 0, 0, 0)\ u'(x, y; r_x, r_y, \tau)}, \tag{3}$$

in the two-dimensional field. Although spatiotemporal parameters are r_x, r_y and τ, only r_x is changed as a variable and the others remain constant. The correlation coefficients are computed at various y.

Figures 9(a) and (b) show the contour maps of two-point correlation coefficients at the reference position of $x = 150$ mm for the diameter ratio of 3 and 5, respectively. As shown in Fig. 9(a), no coherent structure of the flow at $D/d = 3$ can be found except in the neighborhood of the axis of symmetry. In contrast, it can be seen at $D/d = 5$ (Fig. 9(b)) that the regions of the positive and negative correlation coefficients appear periodically in the x-direction; the streamwise length scales of this flow have a same value over the wake, except near $y = 0$ and $y = \pm 90$ mm, where mean velocity gradients in the y-direction dU/dy are nearly equal to 0.

The wake of the torus of $D/d = 5$ exhibits well-organized motion in comparison with $D/d = 3$. This organized structure consists of the inside and outside vortex rings, shed from the torus body and counterrotating with each other, which corresponds to the axisymmetric parallel mode. In order to

confirm this phenomenon, a conditionally averaging method is utilized in the present study. The multi-line measurements with two ultrasonic transducers were carried out and instantaneous velocity profiles at two different locations were sampled almost simultaneously, that is, with a very short interval of 145 ms; one measuring-line is fixed for a reference velocity fluctuation, and the other is moved in the wake. The reference signal is that obtained by rectifying the fluctuating velocity by a band-pass filter, and the time when the reference signal reaches a positive peak is used as a trigger for each cycle.

Figure 10 shows the conditionally averaged vector map ($\langle u \rangle - U_c$, $\langle v \rangle$), where U_c is the convection velocity and estimated at 0.80 U_0 in the preceding section. Vorticities can be deduced from the conditionally averaged velocity field. The vorticity in the x-y plane ω_z is defined as

$$\omega_z = \frac{\partial v}{\partial x} - \frac{\partial u}{\partial y}, \tag{4}$$

and velocity gradients are computed by polynomial approximation. Figure 11 shows a contour map of the vorticity. As shown in Figs. 10 and 11, the vortical structure is symmetric with respect to the axis of symmetry of the torus, and clockwise and counterclockwise vortex rings alternatively arrange in the streamwise direction. A center of the inside vortex rings locates at the radial distance of about 50 mm from the symmetry axis of the torus and a center of the outside vortex rings at the radial distance of about 90 mm. Values of mean velocities in the mainstream direction at the centers of the inside and outside vortex rings, which were utilized as the convection velocity of the vortex ring by Takamoto (1987), are 0.81 U_0 and 0.77 U_0, respectively.

3.2 Flow fields for oblique posture

Figures 12(a)-(f) show the flows at Re = 600 visualized by the electrolytic precipitation method, in which the torus with the diameter ratio of 3 was set up in the oblique postures of $\theta = 0°$, 15°, 30°, 45° and 80°, and the behaviors of the shear layer separated from the torus perimeter are visible by white precipitates. In the axisymmetric case (Fig. 12(a)), the separated shear layer is a cylindrical form rolling up at $x \approx 4d$ (see also in Fig. 4(a)).

For $\theta = 15°$ and 30° (Figs. 12(b) and (c)), the separated flow from the torus forms a cylindrical layer with an axis nearly coincident with the mainstream direction and rolls up at almost the same downstream distance from the leading edge of the torus body. After that, the vortex ring is broken

up into two parts because of an interaction between the outside and inside shear layers. One part exists in the side where the torus rim is inclined upstream, i.e., $y > 0$, and vortex filaments are periodically shed into the wake and have a vortex-loop structure, as shown in a side view for $\theta = 30^\circ$ (Fig. 12(f)). Another part in the downstream-inclined side ($y < 0$) is quasi-periodic at different intervals compared with the upstream-inclined side. For $\theta = 45^\circ$ (Fig. 12(d)) the flow shows almost the same configuration as the preceding case, but the regularity of flow structure in the downstream-inclined side vanishes. For $\theta = 80^\circ$, shown in Fig. 12(e), the intermittent flow through the inside of the torus and the separated flow from the trailing edge were synchronized at a nearly constant interval.

The 3-D maps of power spectra dependent on f and y in the cross section of x = 150 mm are shown in Figs. 13(a)-(d) for the various oblique postures of the torus with $D/d = 5$; a one-dimensional power spectrum $S_{22}(f)$ is obtained by Fourier transforming a time-series data set of 512 points measured by the UVP monitor, where f denotes a frequency. For the axisymmetric flow at $\theta = 0$, the spectral map is symmetric with respect to $y = 0$ and shows two peaks of single frequency of $f \approx 0.34$ Hz at $y \approx \pm 90$ mm. In the case of $\theta = 15^\circ$, the peak frequency in the upstream-inclined side ($y > 0$) increases compared with $\theta = 0$, the one in the downstream-inclined side ($y < 0$) decreases and its power is considerably reduced. In the downstream-inclined side at $\theta = 45^\circ$, no peak is distinguished in the frequency domain, and two ridges become evident in the region of $y < 0$. For $\theta = 80^\circ$, there appears one peak for each spectral ridge with the axis of $y = 0$ between.

Non-dimensional peak frequencies are plotted against the oblique angle in Fig. 14, together with the experimental results of a circular disk by Calbert (1967). When the torus is set with axisymmetric posture (say $\theta = 0$), the Strouhal number is about 0.2. If the torus assumes an oblique posture, the Strouhal numbers in the upstream- and downstream-inclined sides become different from each other; the former increases and the latter decreases with increasing the oblique angle θ up to about $\theta = 30^\circ$. By further increasing θ, the peak in the power spectrum in the downstream-inclined side disappears up to about $\theta = 60^\circ$, and in this range of θ the Strouhal number in the upstream-inclined side is nearly constant or slightly decreases with θ. If θ goes over 60°, the peak in the power spectrum in the downstream-inclined side appears again, and the Strouhal number coincides with the one in the upstream-inclined side which decreases with increasing θ. This variation of the Strouhal number or the peak frequency in the spectrum with respect to the oblique angle θ indicates that the structure of the wake of the inclined torus is altered with θ; four categories can be identified in the situations of θ

$= 0°$, $0° < \theta < 30°$, $30° < \theta < 60°$ and $\theta > 60°$, respectively.

It is found by our previous work for the inclined torus body (Inoue et al., 1995) that a maximum value of lift is obtained at $\theta \approx 60°$, and that the direction of the moment of force acting on the torus is different from each other for $0° < \theta < 70°$ and $70° < \theta < 90°$. These phenomena seem to correlate with the transition of the flow regimes shown in the present experiment.

4 Concluding remarks

The flow structures behind the torus body set with axisymmetric and oblique postures were investigated by the flow visualization technique and UVP monitor. Qualitative explanations were given for the vortical structure in terms of flow visualization. Instantaneous flow pattern, various quantities, including streamwise two-point correlation and power spectral density of fluctuating velocity, and conditionally averaged velocity profiles were analyzed from the data set measured by the UVP monitor. These quantities made clear the structural properties of the wake of the torus.

In the axisymmetric wake at zero inclination, it is confirmed that there were two modes of flow structure. At the lower diameter ratio, the disk mode is observed and consists of the cylindrical shear layer and oblique vortex loop. The streamwise change of these flow structures is clearly found in the time history of the instantaneous velocity profile. At the higher diameter ratio corresponding to the ring wake mode, the counterrotating vortex rings alternately are shed from the torus with regularity. This phenomenon is reflected in the streamwise two-point correlation and conditionally averaged vorticity field. In the case of $D/d = 5$ at $Re \approx 1500$, the convection velocity of the vortex ring is estimated at $0.80\ U_0$.

The vortex shedding frequencies remain almost unchanged for both regimes within the present experiments, and no discrepancy explicitly appears between two wake modes in the shedding frequency. In the ring wake mode, the Strouhal number is nearly constant and slightly decreases as the Reynolds number increases above 1000.

In the oblique postures of the torus, the change in the flow structure with respect to the oblique angle can be made clear by the transverse variations in the power spectrum and behavior of the peak frequencies in the space and frequency domains. The flow patterns can be identified in four categories of $\theta = 0°$, $0° < \theta < 30°$, $30° < \theta < 60°$ and $\theta > 60°$, respectively.

Acknowledgement

The authors wish to express their appreciation to Dr. Ing. Yasushi Takeda of Paul Scherrer Institut for his advice on the UVP system.

References

Amarakoon A M D; Hussey R G; Good B J; Grimsal E G (1982) Drag measurements for axisymmetric motion of a torus at low Reynolds number. Phs. Fluids. 25: 1495-1501

Bearman P W; Wadcock A J (1973) The interaction between a pair of circular cylinders normal to a stream. J. Fluid Mech. 61: 499-511

Blevins R D (1995) Vortex-structure interaction. In: Fluid Vortices. (ed Green, S I). pp 533-574, Netherlands: Kluwer Academic Pub.

Calvert J R (1967) Experiments on the flow past an inclined disk. J. Fluid Mech. 29: 691-703

Goren S L; O'Neill M E (1980) Asymmetric creeping motion of an open torus. J. Fluid Mech. 101: 97-110

Higuchi H; Anderson R W; Zhang J (1996) Three-dimensional wake formations behind a family of regular polygonal plates. AIAA J. 34: 1138-1145

Inoue Y; Okugawa T; Yamashita S (1995) An experimental study on the properties of the 3-dimensional flow around a torus. Proc. 72nd JSME Spring Ann. Meeting. (Tokyo). 3: 63-64

Johnson R E; Wu T Y (1979) Hydromechanics of low-Reynolds-number flow. Part 5. Motion of a slender torus. J. Fluid Mech. 95: 263-277

Leweke T; Provansal M (1995) The flow behind rings: bluff body wakes without end effects. J. Fluid Mech. 288: 265-310

Miau J J; Chiu E G; Chou J H (1992) Laser-sheet flow visualization of the confined wake behind a ring. Fluid Dynamics Research. 9: 255-265

Monson D R (1983) The effect of transverse curvature on the drag and vortex shedding of elongated bluff bodies at low Reynolds number. Trans. ASME J. Fluids Eng. 105: 308-322

Sakamoto H; Haniu H (1990) A study on vortex shedding from spheres in a uniform flow. Trans. ASME J. Fluids Eng. 112: 386-392

Takamoto M (1987) A study of the wake structure behind bluff rings. Bull. National Research Laboratory of Metrology. 36: 445-537

Takeda Y (1995) Velocity profile measurement by ultrasonic Doppler method. In: Experimental Thermal and Fluid Science. Vol. 10, pp 444-453, New York: Elsevier Sci. Inc.

Tobak M; Peake D J (1982) Topology of three-dimensional separated flows. Ann. Rev. Fluid Mech. 14: 61-85

Williamson C H K (1995) Vortex dynamics in the wake of a cylinder. In: Fluid Vortices. (ed Green, S I). pp 155-234, Netherlands: Kluwer Academic Pub.

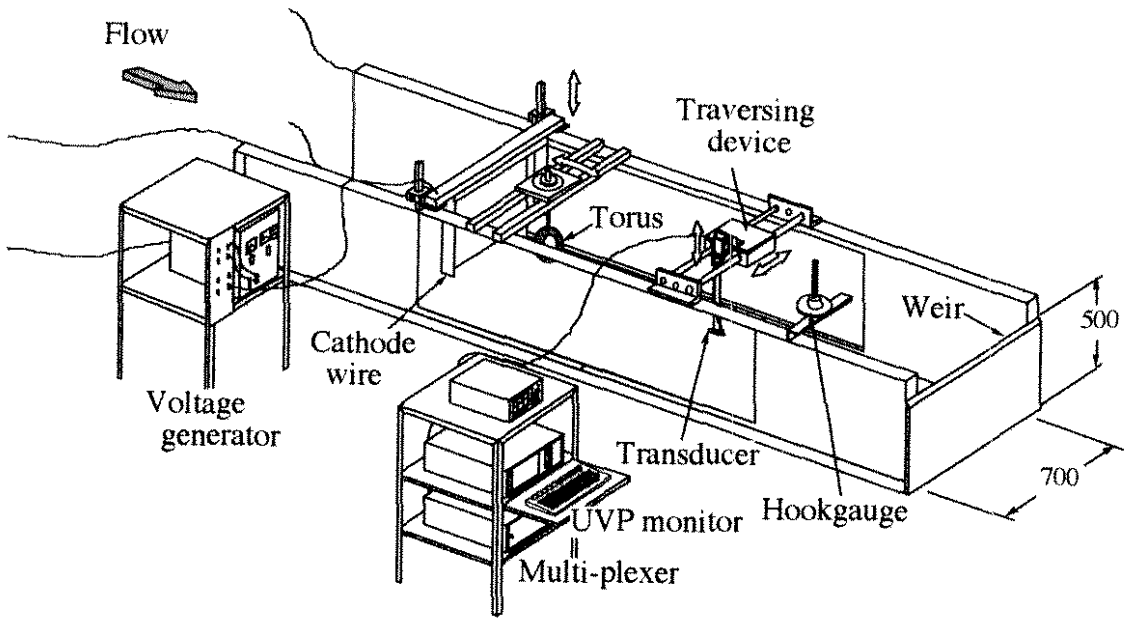

Fig. 1. Sketch of the test section

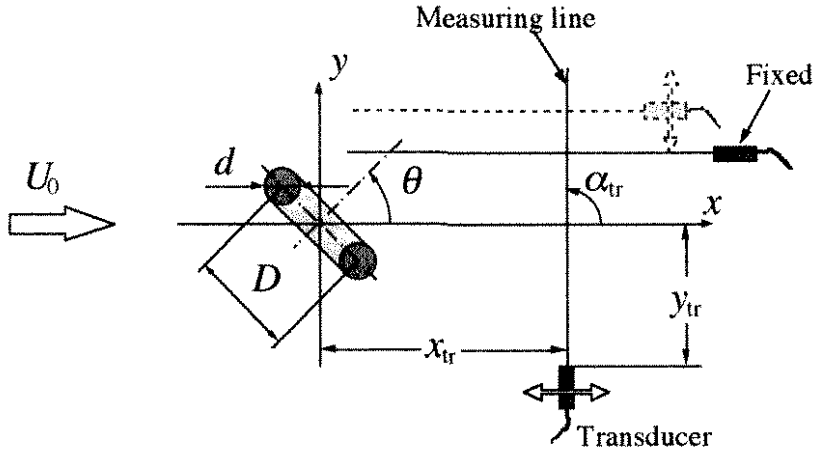

Fig. 2. Flow field and coordinate system

Table 1. Specifications of UVP measurement

	x-direction	*y*-direction	Ref. TRD
α_{tr} (deg)	180	90	180
x_{tr} (mm)	590	90 ~ 420	690
y_{tr} (mm)	-198 ~ 198	273	45
ξ_{st} (mm)	20	15	←
ξ_{ch} (mm)	4.44	3.70	←
Emission voltage	150 V		
Basic frequency	4 MHz		
Pulse repetition frequency	978 Hz		
Number of pulse repetition	16		
Cycles per pulse	4		

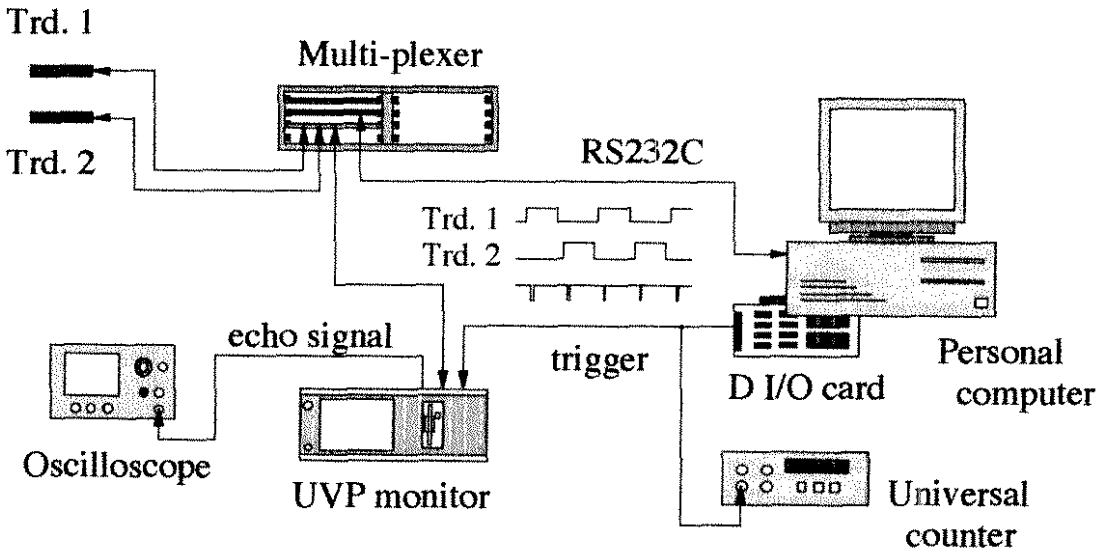

Fig. 3. Multi-line measurement system

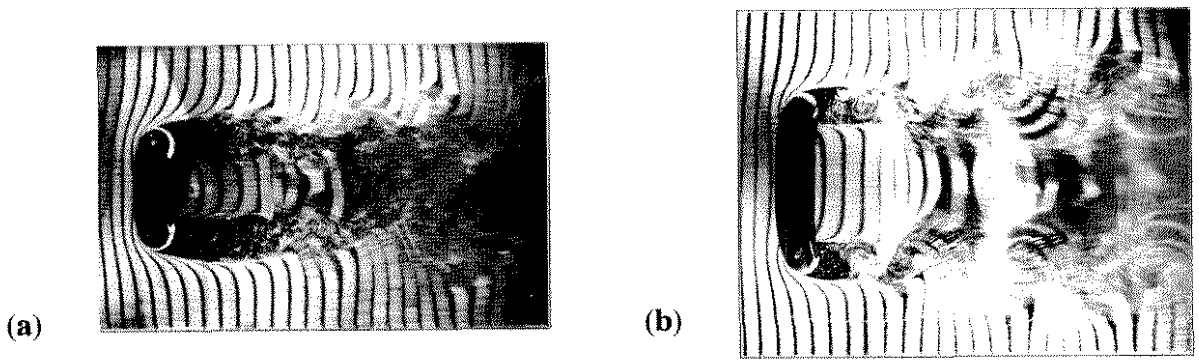

Fig. 4. Flow visualizations at $\theta = 0°$ by the hydrogen bubble method. (a) $D/d = 3$; (b) $D/d = 5$.

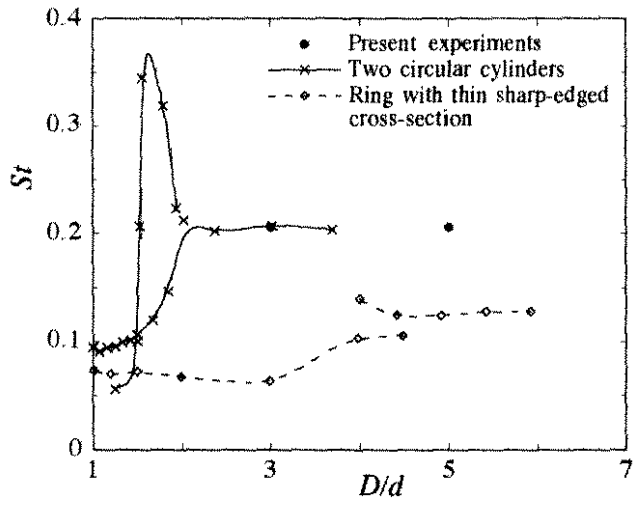

Fig. 5. Variation of Strouhal number with geometrical parameter *D/d*

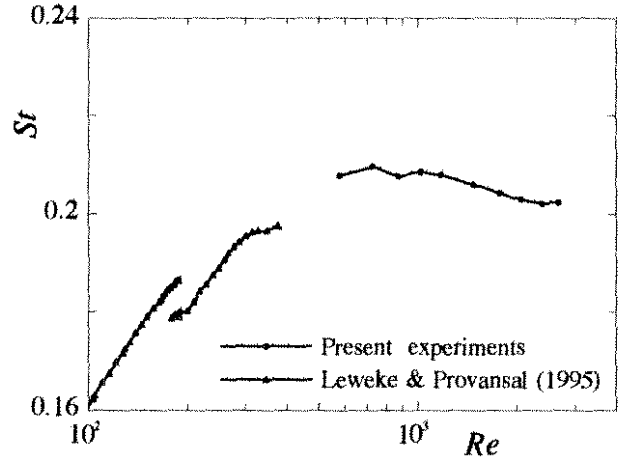

Fig. 6. Strouhal-Reynolds number relationship in the ring wake mode

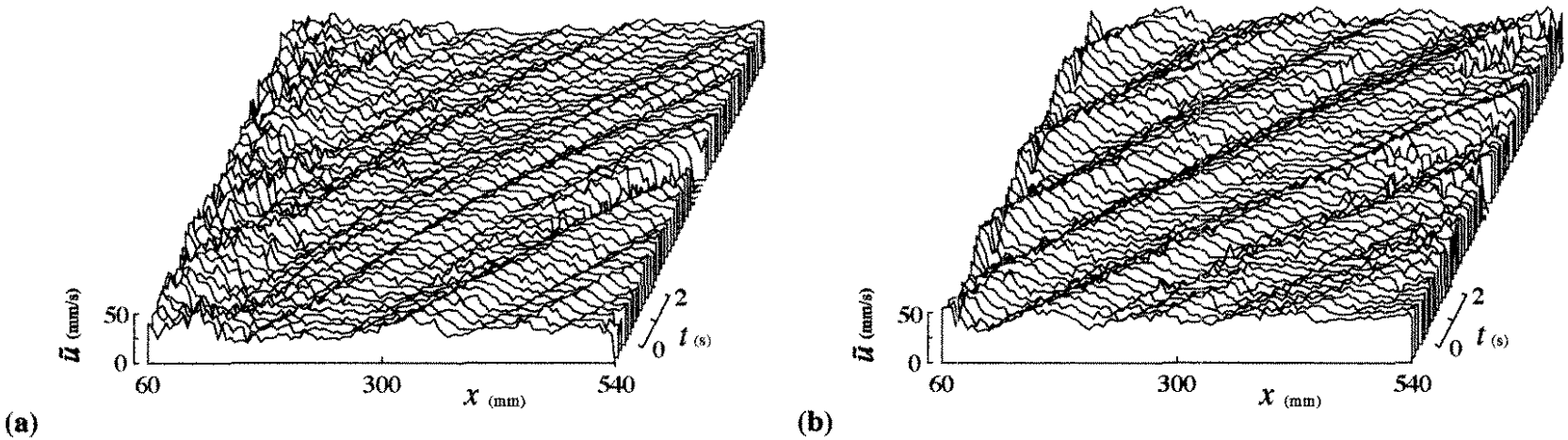

Fig. 7. Time history of the streamwise distribution of velocity component $\tilde{u}$. (a) $D/d = 3$; (b) $D/d = 5$.

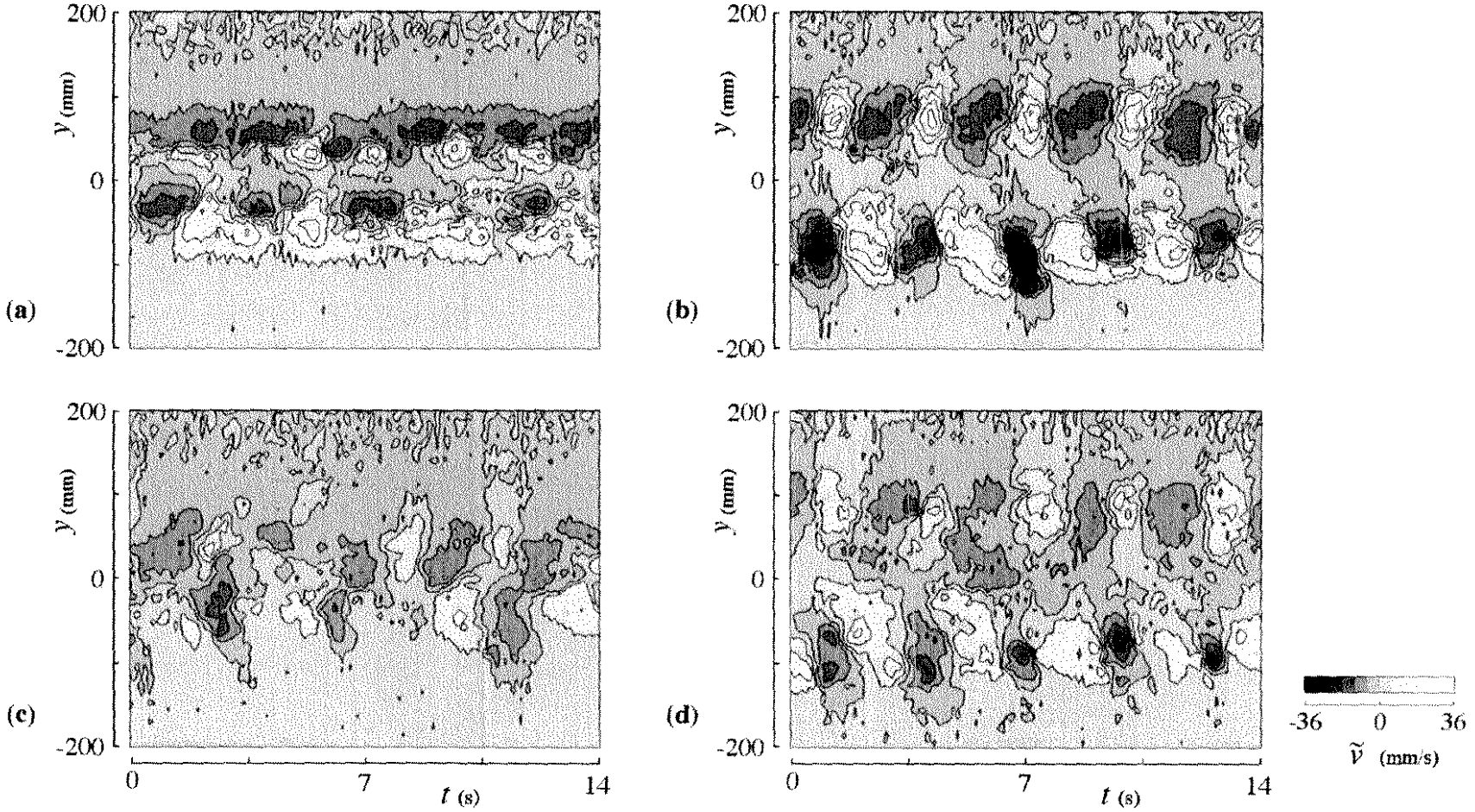

Fig. 8. Velocity contour maps in the y-t field of component $\tilde{v}$. (a) $D/d = 3$, $x = 150$ mm; (b) $D/d = 5$, $x = 150$ mm; (c) $D/d = 3$, $x = 300$ mm; (d) $D/d = 5$, $x = 300$ mm.

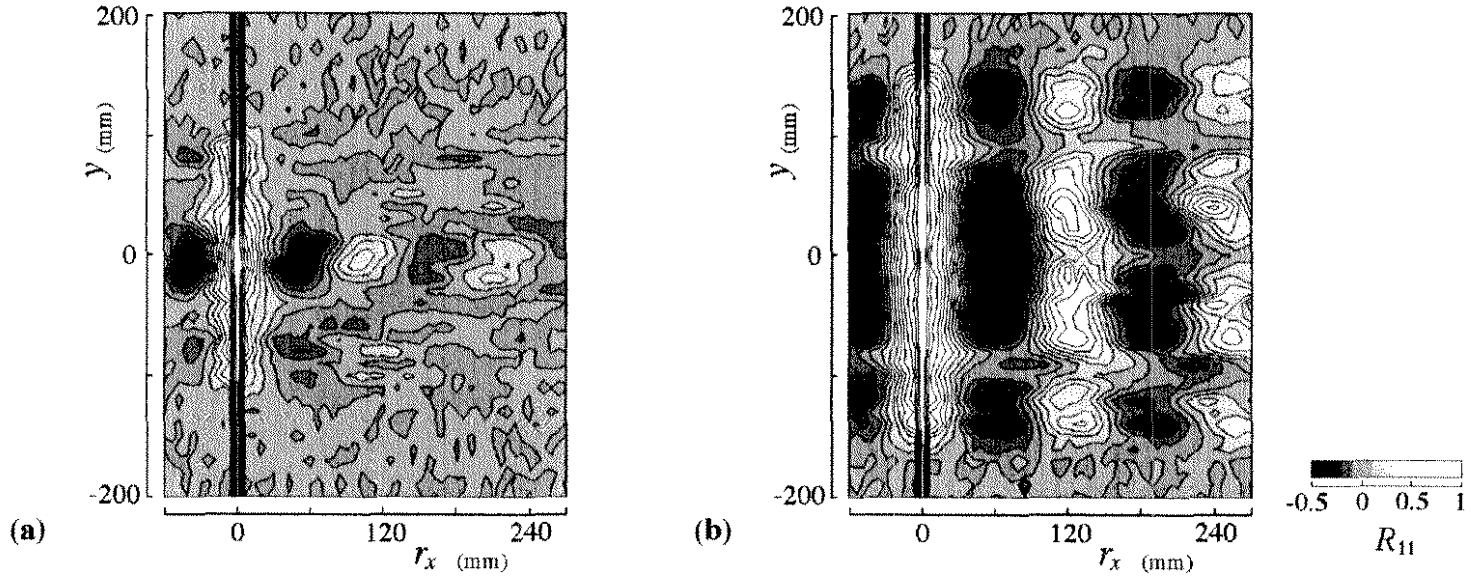

Fig. 9. Contour maps of the two-point correlation coefficient in the streamwise direction. (a) $D/d = 3$; (b) $D/d = 5$.

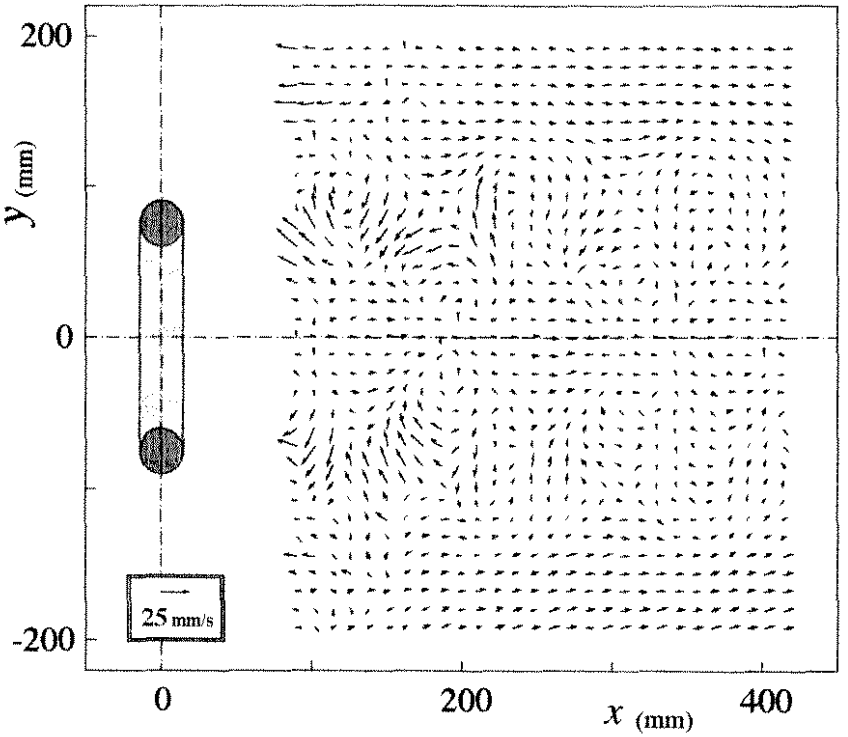

Fig. 10. Vector map of conditionally averaged velocity

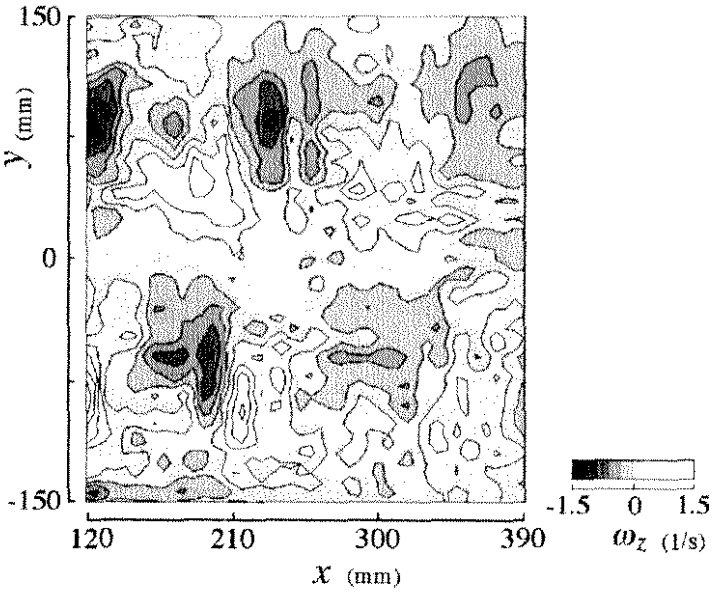

Fig. 11. Contour map of vorticity

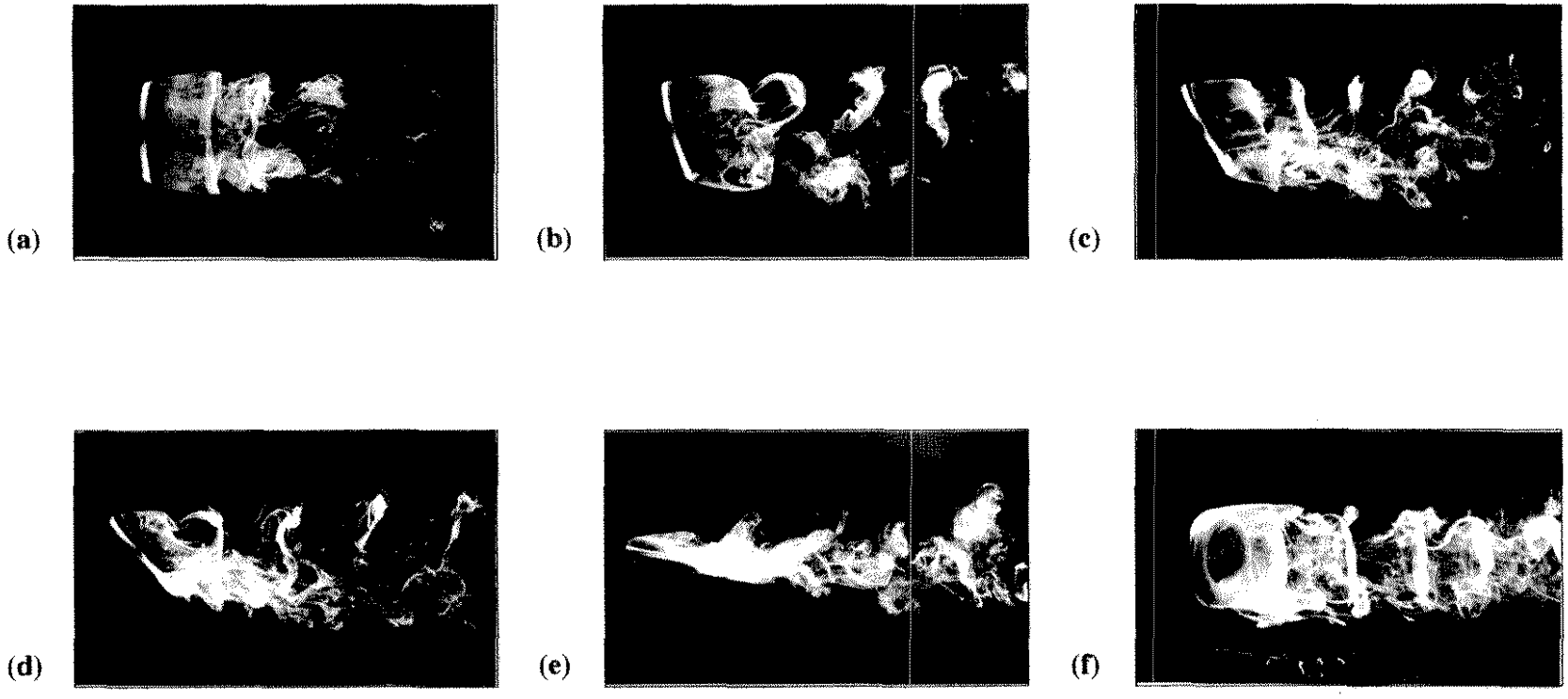

Fig. 12. Flow visualizations of the torus with $D/d = 3$ by the electrolytic precipitation method. Top-views at (a) $\theta = 0°$; (b) $\theta = 15°$; (c) $\theta = 30°$; (d) $\theta = 45°$; (e) $\theta = 80°$, and (f) side-view at $\theta = 30°$.

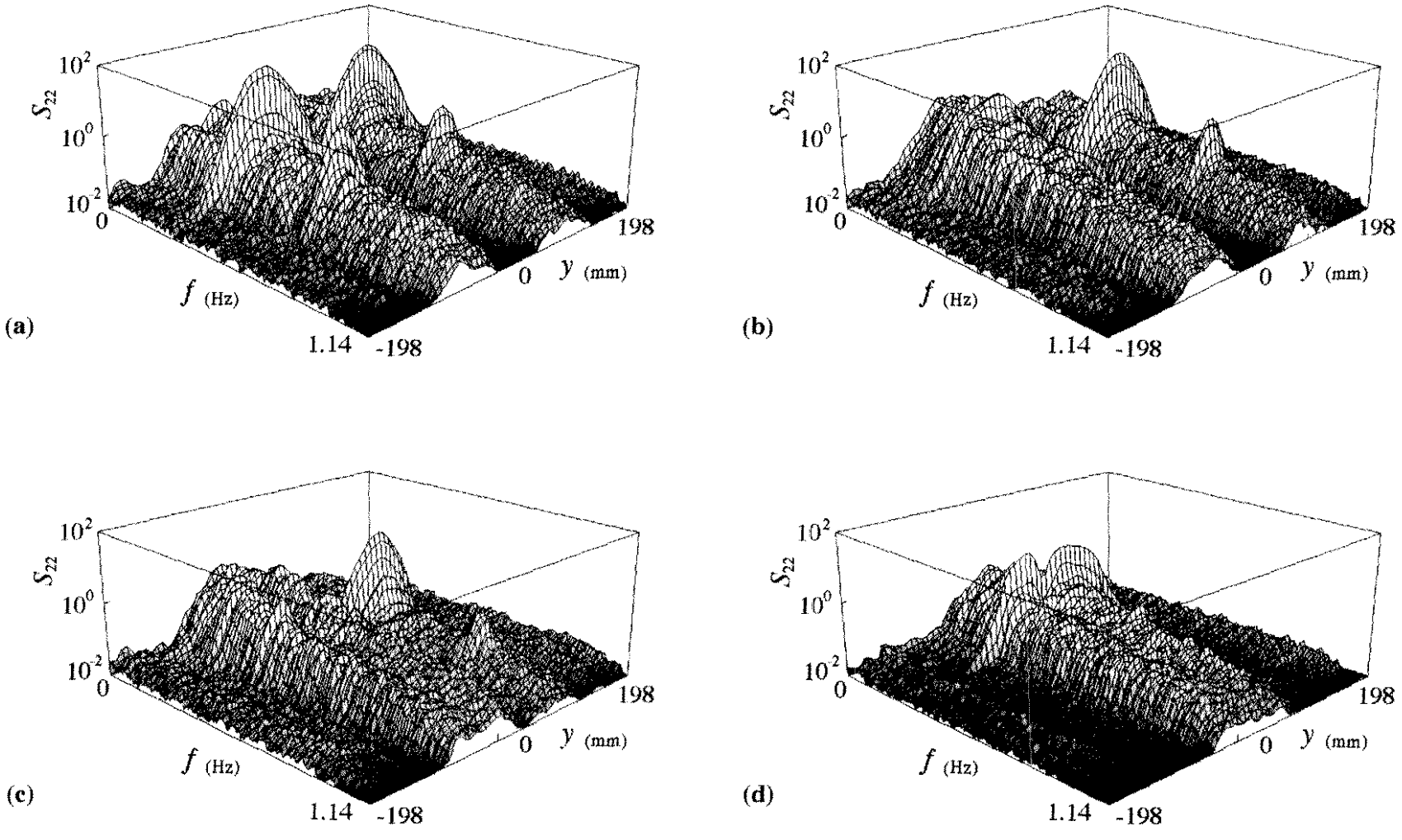

Fig. 13. Transverse variations in the power spectrum of the velocity component v in the wake of the torus with $D/d = 5$. (a) $\theta = 0°$, (b) $\theta = 15°$, (c) $\theta = 45°$ and (d) $\theta = 80°$.

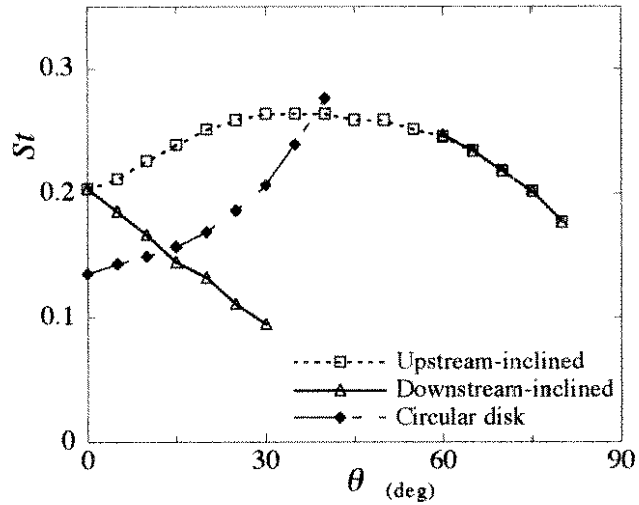

Fig. 14. Variation of Strouhal number with oblique angles θ